Drift Recovery and Station Keeping Results for the Historic CanX-4/CanX-5 Formation Flying Mission

Josh Newman
Supervisor: Dr. Robert E. Zee
University of Toronto Institute for Aerospace Studies, Space Flight Laboratory
4925 Dufferin Street, Toronto, Ontario, Canada, M3H5T6
jnewman@utias-sfl.net

ABSTRACT

Specialized drift recovery and station keeping algorithms were developed for the Canadian Advanced Nanospace eXperiments 4 and 5 (CanX-4 & CanX-5) formation flying mission (launched 30 June 2014), and successfully verified on orbit. These algorithms performed almost exactly according to predictions. The highly successful CanX-4 and CanX-5 formation flying demonstration mission was completed in November 2014, ahead of schedule.

CanX-4 & CanX-5 are a pair of identical formation flying nanosatellites that demonstrated autonomous sub-metre formation control, with relative position knowledge of better than 10 cm and control accuracy of less than one metre at ranges of 1000 to 50 metres. This level of performance has never before been seen on nanosatellite class spacecraft to the author's knowledge. This capability is crucial to the future use of coordinated small satellites in applications such as sparse aperture sensing, interferometry, ground moving target indication, on-orbit servicing or inspection of other spacecraft, and gravitational and magnetic field science. Groups of small, relatively simple spacecraft can also replace a single large and complex one, reducing risk through distribution of smaller instruments, and saving money by leveraging non-recurring engineering costs.

To facilitate the autonomous formation flight mission, it was a necessary precondition that the two spacecraft be initially brought within a few kilometres of one another, with a low relative velocity. Complicating this was the fact that the CanX-4 and CanX-5 spacecraft were released separately from their shared launch vehicle, drifting thousands of kilometres apart in the short time it took to fully commission one spacecraft. Therefore, a system to calculate fuel-efficient recovery trajectories and produce the corresponding spacecraft commands was required, another first on the nanosatellite scale. This system was also extended to provide station keeping capabilities in the time between individual formation experiments, to keep the spacecraft safely separated without allowing their distance to grow large again.

I. INTRODUCTION

The use of multiple, coordinated spacecraft, often in relatively close proximity to one another, also known as formation flight, is a critical field in the future of space flight. Its applications range from synthetic aperture radar and optical interferometry, to on-orbit servicing of other spacecraft, to gravitational and magnetic field science. Groups of small, relatively simple spacecraft can also potentially replace a single large and complex one, reducing risk through distribution of instruments, and saving money by leveraging non-recurring engineering costs. Performance of the entire formation can be gradually built up over several launches, maintained over time with replacement units when others fail, or allowed to gracefully degrade.

Nanosatellites represent the extreme application of formation flight's benefits, using the most cost effective, mass-producible spacecraft available, capable of being deployed en masse from a single launch. It is only in the last few years that nanosatellite technology has matured to the point where this is possible.

Work towards autonomous formation flight of nanosatellites has been ongoing at the University of Toronto Institute for Aerospace Studies-Space Flight Laboratory (UTIAS-SFL) for several years. This work can be traced back to the CanX-2 spacecraft, launched in 2008, which demonstrated a number of technologies required for formation flight, including a cold-gas propulsion system and precision GPS receiver, in a 3U form factor [1]. CanX-4 and CanX-5 represent the latest efforts in the field, and have set the bar for the state-of-the-art in nanosatellite formation flying [2] with the completion of their primary mission in November 2014.

As the autonomous formation flying algorithms relied upon an Inter-Satellite Link (ISL) between the spacecraft, it was required that the two spacecraft be brought within a few kilometres of one another. Had the spacecraft been ejected from their launch vehicle while still attached, and only separated after being fully commissioned, this would be trivial. To meet launch vehicle requirements, however, the spacecraft were

ejected separately and allowed to drift apart until one spacecraft was ready to begin orbit phasing manoeuvres.

To meet these requirements, a system that plans recovery trajectories independent of the ISL and over large distances was required. The small volume available inside these nanosatellites limits the amount of propellant that can be carried onboard, and consequently these manoeuvres would need to be performed with as little fuel as possible. Finally, this system would also be extended to meet stationkeeping requirements, maintaining safe spacecraft separation between formation flight experiments.

II. CANX-4 & CANX-5

Generic Nanosatellite Bus

CanX-4 and CanX-5 (CanX-4&5) are identical nanosatellites, each with a mass of just over 6 kg, based on the Generic Nanosatellite Bus (GNB) developed by SFL. The GNB is a 20 x 20 x 20 cm cube, designed with mission flexibility in mind. In addition to formation flight, the GNB has been used for the BRIght Target Explorer (BRITE) constellation of stellar astronomy spacecraft, and numerous automatic identification system (AIS) spacecraft used to track maritime traffic [2].

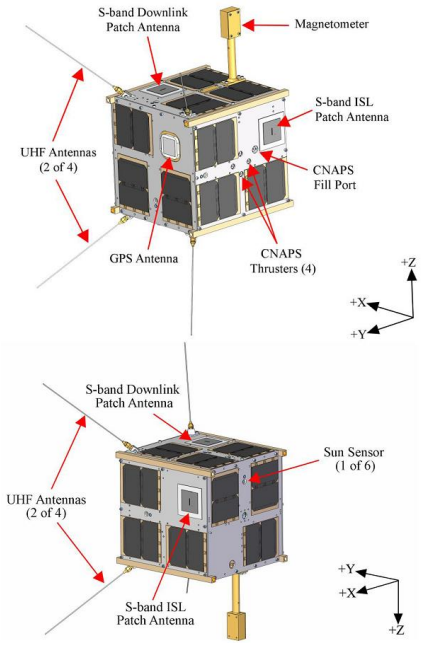

Figure 1: CanX-4 layout (CanX-5 identical) [3].

Attitude and Orbital Determination and Control

CanX-4&5 each carry a suite of attitude sensors and actuators for full three-axis attitude determination and control. These include sun and rate sensors, a three-axis magnetometer mounted on an external boom, three orthogonally mounted magnetorquers and three reaction wheels. A NovAtel OEMV-1G Global Position System (GPS) receiver and surface-mounted antenna is used to collect high precision information on the spacecraft's orbital state.

The Canadian Nanosatellite Advanced Propulsion System (CNAPS) cold gas propulsion system provides orbital control for drift recovery, station keeping, and formation control and reconfiguration. Using four nozzles and 260 g of liquid sulphur hexafluoride (SF_6) as a propellant, the system provides a specific impulse greater than 40 s and a total impulse capability of 100 N s. SF_6 was chosen for its high storage density and vapour pressure which makes the system self-pressurizing, as well as its inert properties, making it both safe to handle and compatible with most materials [4]. Thrust levels range from 12.5 to 50 mN, depending on thruster selection. As the four nozzles are located on a single face of the spacecraft bus, thruster selection also allows the system to be used for momentum management, with specific nozzles autonomously selected to reduce momentum build-up on the spacecraft. This requires that the attitude control system be able to quickly slew the spacecraft during formation flight, such that the thrusters point in the correct direction prior to thrusting.

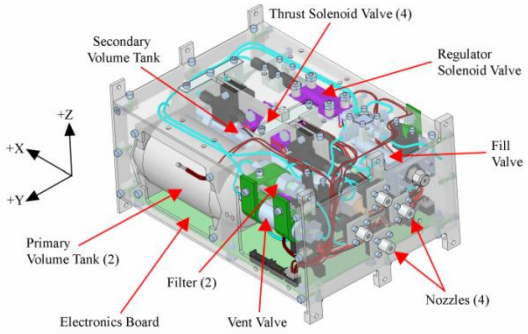

Figure 2: Interior view of CNAPS [4].

CanX-4&5 Formation Flying Mission

Four different formations make up the precision formation flight portion of the mission. These are a 1000 and 500 m along-track orbit (ATO), and a 100 and 50 m projected circular orbit (PCO) [3]. In an along-track orbit, one spacecraft simply follows directly behind the other. In terms of orbital elements, the two spacecraft are in an identical state, except for a small difference in true anomaly. In a projected circular orbit, one spacecraft appears to trace out a circle around the other spacecraft over the course of an orbit. This is accomplished using a differential inclination (for out-of-orbital-plane motion) and eccentricity (for in-orbital-plane motion). Relative semi-major axis is kept as close to zero as possible, as varying this element would create

an undesirable secular along-track drift between the spacecraft [5].

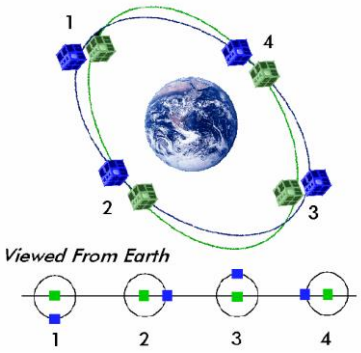

Figure 3: Projected circular orbit as seen from Earth (left) and as seen by an external observer (right), over one orbit.

The requirements placed on formation control are, to the author's knowledge, the most stringent ever on a satellite of this size. Formation control error is required to be less than 1 m, and relative position and velocity estimation errors are required to be less than 1 m and 1 mm/s, 2σ, respectively. The nominal mission called for ten orbits in each of the four formations, with a possibility to extend the mission to fifty orbits in some or all of the formations, or to perform other formations such as the J_2- invariant relative orbit. CanX-4&5 use a standard chief/deputy architecture, where one spacecraft, denoted the "chief", remains passive, while the "deputy" performs all of the thrusts required to achieve a desired relative state.

III. DRIFT RECOVERY CONTROLLER DESIGN

The goal of the Drift Recovery and Station Keeping (DRASTK) system is to place one spacecraft directly behind the other, with as close to zero relative motion as possible. In mean orbital element terms, this means going from an initial state, with the spacecraft drifting under the effects of differential elements, to a final state where the elements of one spacecraft match those of the other, except for a small difference in the true anomaly. It is therefore important to understand how each of these elements evolves, either over time or by applying a control force.

Time-Varying Orbital Elements Including J_2

While all orbital elements see some drift due to the oblateness of the Earth, also known as J_2, only the right ascension of the ascending node (RAAN), argument of perigee, and mean anomaly experience secular changes over time [7]. Semi-major axis, inclination, and eccentricity experience short- and long-term periodic oscillations.

In the following, the semi-major axis will be given by a, the eccentricity by e, the inclination by i, the argument of perigee by ω, the RAAN by Ω, and the mean anomaly by M. Furthermore, the orbital radius is given by r, the coefficient of the second spherical harmonic of Earth's gravity, 1.08263 x 10^{-3} will be given by J_2, the standard gravitational parameter of the Earth will be given by μ and the Earth's radius, 6371 km, will be given by $R_\oplus$. The following definitions also help to simplify the algebra:

$$n = \sqrt{\frac{\mu}{a^3}}$$
$$\eta = \sqrt{1 - e^2}$$
$$p = r(1 + e\cos M)$$
$$G = -\frac{3}{2}J_2\left(\frac{R_\oplus}{a\eta^2}\right)^2$$

where n is the mean orbital motion and p is the semilatus rectum. The RAAN, argument of perigee, and mean anomaly experience secular drifts given by:

$$\dot{\Omega} = Gn\cos i \quad (1)$$
$$\dot{\omega} = \frac{1}{2}G\eta(1 - 5\cos^2 i) \quad (2)$$
$$\dot{M} = n\left(1 + \frac{1}{2}G\eta(1 - 3\cos^2 i)\right) \quad (3)$$

Along-Track Drift Rates

The sum of the drifts in argument of perigee and mean anomaly is the precession of the argument of latitude:

$$\dot{\lambda} = \dot{\omega} + \dot{M} \quad (4)$$

More importantly, the relative secular along-track drift rate between two spacecraft, or the speed at which they are separating, is given by:

$$\delta\dot{\lambda} = \dot{\lambda}_d - \dot{\lambda}_c \quad (5)$$

where the d and c subscripts refer to the deputy and chief spacecraft, respectively.

In general, the state vector containing all six of the deputy's elements can be written as:

$$\boldsymbol{\epsilon_d} = \boldsymbol{\epsilon_c} + \delta\boldsymbol{\epsilon} \quad (6)$$

where $\delta\boldsymbol{\epsilon}$ is the differential element vector. Assuming the relative elements are small, as is usually the case for two spacecraft off of the same launch vehicle, the in-plane secular drift rate of the Deputy can be expanded as a Taylor series [7]:

$$\begin{aligned}\dot{\lambda}_d &= \dot{\lambda}(\boldsymbol{\epsilon_d}) \\ &= \dot{\lambda}(\boldsymbol{\epsilon_c} + \delta\boldsymbol{\epsilon}) \\ &= \dot{\lambda}(\boldsymbol{\epsilon_c}) + \left.\frac{\partial\dot{\lambda}}{\partial\boldsymbol{\epsilon}}\right|_{\boldsymbol{\epsilon_c}} \delta\boldsymbol{\epsilon} + \frac{1}{2}\delta\boldsymbol{\epsilon}^T \left.\frac{\partial^2\dot{\lambda}}{\partial\boldsymbol{\epsilon}^2}\right|_{\boldsymbol{\epsilon_c}} \delta\boldsymbol{\epsilon} + \cdots\end{aligned} \tag{7}$$

Ignoring any terms second order or above, the relative secular drift rate in the orbital plane is:

$$\begin{aligned}\delta\dot{\lambda} &= \dot{\lambda}_d - \dot{\lambda}_c \\ &= \left(\dot{\lambda}(\boldsymbol{\epsilon_c}) + \left.\frac{\partial\dot{\lambda}}{\partial\boldsymbol{\epsilon}}\right|_{\boldsymbol{\epsilon_c}} \delta\boldsymbol{\epsilon}\right) - \dot{\lambda}(\boldsymbol{\epsilon_c}) \\ &= \left.\frac{\partial\dot{\lambda}}{\partial\boldsymbol{\epsilon}}\right|_{\boldsymbol{\epsilon_c}} \delta\boldsymbol{\epsilon}\end{aligned} \tag{8}$$

or, to be more explicit, since $\dot{\lambda}$ is dependent only on semi-major axis, eccentricity, and inclination, and not argument of perigee, RAAN, or mean anomaly (Equations (2) and (3)):

$$\delta\dot{\lambda} = \left.\frac{\partial\dot{\lambda}}{\partial a}\right|_{\boldsymbol{\epsilon_c}} \delta a + \left.\frac{\partial\dot{\lambda}}{\partial e}\right|_{\boldsymbol{\epsilon_c}} \delta e + \left.\frac{\partial\dot{\lambda}}{\partial i}\right|_{\boldsymbol{\epsilon_c}} \delta i \tag{9}$$

The partial derivatives of which are given by:

$$\begin{aligned}\frac{\partial\dot{\lambda}}{\partial a} &= -\frac{3n}{2a} - \frac{7Gn}{4a}\left(1 - 5\cos^2 i + \eta(1 - 3\cos^2 i)\right) \\ \frac{\partial\dot{\lambda}}{\partial e} &= -\frac{2nGe}{\eta^2}(1 - 5\cos^2 i) + \frac{3nGe}{2\eta}(1 - 3\cos^2 i) \\ \frac{\partial\dot{\lambda}}{\partial i} &= \frac{Gn}{2}\sin 2i\,(5 + 3\eta)\end{aligned} \tag{10}$$

Solving Equation (9) gives the relative in-plane drift rate. The current in-plane angular separation can be determined from navigational sensors such as GPS. Then, for a given chief state and set of relative semi-major axis, the time until the two spacecraft cross in the along-track direction can be solved for:

$$T = \frac{\delta\lambda}{\delta\dot{\lambda}} \tag{11}$$

Nodal Precession

Recall from Equation (1) that the RAAN of any non-equatorial Earth-orbiting spacecraft will experience secular drift as a function of its semi-major axis, inclination, and eccentricity, in an effect called nodal precession. For nearly circular orbits, the eccentricity effect can be neglected. Therefore, two spacecraft with a differential semi-major axis and inclination may experience different magnitudes of nodal precession, which manifests itself as a relative cross-track motion, with a period of one orbit, which steadily increases in magnitude over time.

For a given chief and deputy state and time of flight, the future relative RAAN can be calculated. Conversely, for a given chief state and time of flight, a relative inclination can be found to bring the future relative RAAN to a desired value (such as 0) for any arbitrary relative semi-major axis, or a relative semi-major axis can be found to do the same for any arbitrary inclination.

Higher-Order Effects on e and ω

Beyond J_2, higher order perturbations also effect the orbital elements, however in most cases the effects are insignificant. The exceptions are eccentricity and argument of perigee, which see a large change with the addition of J_3, especially when the eccentricity is very small. These effects are described in detail by Kozai in [8], and Figure 4 illustrates the effect for an orbit representative of CanX-4&5. Note that with the inclusion of J_3, the argument of perigee maintains the same overall period, but no longer changes in a linear fashion. Instead, as the mean eccentricity gets very low (roughly < 0.001), the argument of perigee begins to change very rapidly. If the eccentricity is even smaller, the argument of perigee will no longer move the full 360 degrees around the Earth, but oscillate about 90 degrees [8]. In either case, these nonlinearities mean that the relative eccentricity and argument of perigee between the chief and deputy will also vary nonlinearly.

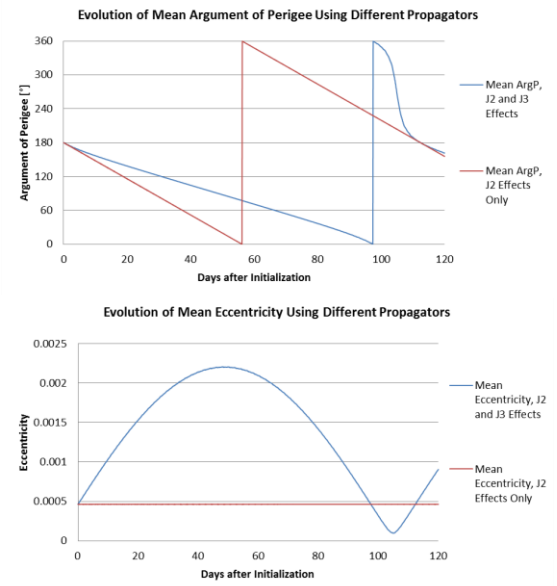

Figure 4: mean eccentricity and argument of perigee over time using J_2 and J_3 propagators

Impulsive Control of Orbital Elements

Perturbations to the classical orbital elements in the presence of perturbing accelerations are given by Gauss' variational equations [8]. Traditionally, these are written with the control expressed as an acceleration, and the elements changing over a time dt. Assuming that these accelerations take place over a short period of time, and assuming a constant spacecraft mass throughout, the variational equations can be rewritten using more intuitive and convenient velocity change, or ΔV quantities:

$$da = \frac{2a^2}{\sqrt{\mu a(1-e^2)}}\left[e \sin M \, \Delta V_R + \frac{p}{r}\Delta V_{AT}\right] \quad (12)$$

$$de = \sqrt{\frac{a(1-e^2)}{\mu}}\left[\sin M \, \Delta V_R + \frac{r(2\cos M + e(1+\cos^2 M))}{p}\Delta V_{AT}\right] \quad (13)$$

$$di = \sqrt{\frac{a(1-e^2)}{\mu}}\frac{r\cos(\lambda)}{p}\Delta V_Z \quad (14)$$

$$d\Omega = \sqrt{\frac{a(1-e^2)}{\mu}}\frac{r\sin(\lambda)}{p\sin i}\Delta V_Z \quad (15)$$

$$d\omega = \sqrt{\frac{a(1-e^2)}{\mu}}\left[\frac{-\cos M}{e}\Delta V_R + \frac{r(2+e\cos M)\sin M}{p\, e}\Delta V_{AT} - \frac{r\sin(\lambda)}{p\tan i}\Delta V_Z\right] \quad (16)$$

where ΔV_{AT}, ΔV_R, ΔV_Z are changes in velocity in the along-track, radial, and out-of-plane directions, respectively. Note that all absolute elements are those of the chief spacecraft.

Control Strategy

A useful consequence of Equations (12) to (16) is that, if multiple elements need to be corrected, their manoeuvres can be combined in to a single impulse to save fuel. For example, in [9], the six elements were combined in to three pairs, which were: semi-major axis/eccentricity, inclination/ RAAN, and argument of perigee/mean anomaly. However, as discussed earlier in this section, if an extended period of time is available, the relative argument of latitude and RAAN can be manipulated using changes to other elements. Because the argument of latitude is the sum of the argument of perigee and mean anomaly, some additional active control will be required to match the argument of perigees. Therefore, the four orbital elements that need to be controlled are: semi-major axis, eccentricity, argument of perigee, and inclination. Eccentricity sees the greatest change with an along-track thrust at apogee or perigee, while semi-major axis is most effectively corrected with an along-track thrust at perigee, however for nearly circular orbits semi-major axis is not sensitive to the mean anomaly at the time of the thrust. Argument of perigee correction also benefits the most from along-track thrusts; however these are optimally performed at a mean anomaly of 90 or 270 degrees. Inclination can only be changed with an out-of-plane thrust, and is most effectively done when the argument of latitude is 0 or 180 degrees (as the spacecraft crosses the equatorial plane). One additional consideration is that the semi-major axis and inclination should be changed at the same time in order to simplify the relative nodal precession calculations and the timing of their correction is critical to ensuring the rendezvous occurs as predicted, while the argument of perigee and eccentricity corrections can occur at any time. Therefore, the semi-major axis and inclination constitute one element pair, and the argument of perigee and eccentricity make up the second.

Then, the ΔV_{AT} to perform the semi-major axis change is:

$$\Delta V_{AT} = (a_1 - a_0)\frac{r\sqrt{\mu a(1-e^2)}}{2a^2 p} \quad (17)$$

where a_0 and a_1 are the deputy's initial and desired semi-major axis, respectively, and all other elements are those of the chief spacecraft. Likewise, the ΔV_Z to perform the inclination change is:

$$\Delta V_Z = (i_1 - i_0)\frac{p}{r\cos(\lambda)}\sqrt{\frac{\mu}{a(1-e^2)}} \quad (18)$$

The total ΔV of the manoeuvre is simply the root of the sum of the squares of these two values. As mentioned previously, to minimize fuel costs, this thrust would optimally occur when the argument of latitude λ is 0 or 180 degrees, when the spacecraft crosses the equatorial plane. As the CNAPS propulsion system would only accept commands that resulted in a ΔV of less than about 5 cm/s, it was expected that this manoeuvre would have to be divided up amongst many orbits, with up to 2 thrusts per orbit. However, as an additional fuel saving measure, the possibility to only thrust once per orbit was also included, if that would also result in a favourable change to the eccentricity and argument of perigee. Thrusting twice per orbit, 180 degrees in mean anomaly apart, would always result in zero net change to argument of perigee and eccentricity. While only thrusting once per orbit would result in more orbits being required to complete the manoeuvre, this

cost would be small compared to the value of the propellant conserved.

The mean anomaly that results in the smallest thrust to correct the eccentricity and argument of perigee is not immediately obvious from looking at Equations (13) and (16), as it depends on the values of the two relative elements, and these will change over time. To find the optimal manoeuvre time, the following function is minimized over the mean anomaly:

$$\begin{aligned} A &= \sqrt{\frac{a(1-e^2)}{\mu}}\begin{bmatrix} 2\cos M & \sin M \\ \frac{2\sin M}{e} & -\frac{\cos M}{e} \end{bmatrix} \\ C &= \begin{bmatrix} \delta e \\ \delta\omega \end{bmatrix} \\ \Delta V_{e,\omega} &= |A^{-1}C| \end{aligned} \tag{19}$$

Orbit Phasing Trajectory Analysis

In the previous section, the method of going from a post-launch vehicle ejection trajectory to a relative orbit phasing trajectory was discussed, but not how that trajectory is chosen. This requires locating the minimum of a fuel cost function with multiple terms. That cost function is written as:

$$\Delta V_{cost} = \Delta V_{a,i_1} + \Delta V_{a,i_2} + \Delta V_{e,\omega} + \Delta V_{Time} \tag{20}$$

$\boldsymbol{\Delta V_{a,i_1}}$ is the cost of bringing the deputy spacecraft from its initial, drifting state after launch vehicle ejection to the desired one that will result in rendezvous at the desired time. Knowing the chief's state and range to the deputy, and choosing a deputy semi-major axis for the return coast phase $a_{d,1}$, Equation (11) gives a time to rendezvous T. Then, to alter the deputy's nodal precession to bring it in phase with the chief at the time of rendezvous, the desired inclination is found by rearranging Equation (1):

$$i_{d,1} = \cos^{-1}\left(-\frac{2\delta\Omega(1-e^2)}{3TJ_2R_\oplus}\sqrt{\frac{a^7}{\mu}}\right) \tag{21}$$

Then, the root sum squared of the results of Equations (17) and (18) give $\Delta V_{a,i_1}$.

$\boldsymbol{\Delta V_{a,i_2}}$ is the cost of bringing the deputy's semi-major axis and inclination from the orbit phasing coast state, $a_{d,1}$ and $i_{d,1}$, to the final state where these elements match those of the chief spacecraft, a_c and i_c, again using Equations (17) and (18).

$\boldsymbol{\Delta V_{e,\omega}}$ is the eccentricity and argument of perigee correction cost, after the first set of manoeuvres have put the deputy on its orbit phasing trajectory. As described in the previous section, the along-track thrusts used to change the semi-major axis can also be used to perform a significant amount of the eccentricity and argument of perigee correction. To model this benefit, a term called the eccentricity/argument of perigee savings fraction, or $S_{e,\omega}$, is introduced:

$$\Delta V_{e,\omega} = \Delta V_{e,\omega_0} - S_{e,\omega}\Delta V_{AT_1} \tag{22}$$

where $\Delta V_{e,\omega_0}$ is the cost to correct the eccentricity and argument of perigee if $\Delta V_{a,i_1}$ did not occur, and ΔV_{AT_1} is the along-track component of $\Delta V_{a,i_1}$. Through simulation, the $S_{e,\omega}$ has been found to be approximated by:

$$S_{EccArgP} = \left|\sin\left(2\omega\frac{\pi}{\frac{\pi}{2}+A}+\frac{\pi}{2}+A\right)\right| \tag{23}$$

where A is the amplitude of the mean argument of perigee's oscillation, as recall from earlier that in cases with extremely low eccentricity, the argument of perigee will oscillate about 90 degrees rather than travel the full 360 degrees about the Earth.

ΔV_{Time} represents the thrusting capability lost due to fuel leakage over time. Having already determined the time to rendezvous for a given relative semi-major axis, this value is obtained by multiplying the time with a user-defined time value for fuel, which in the case of CanX-4&5 is an experimentally determined leak rate, with the only further complication being the conversion of leak rate from mass over time to ΔV over time. This is done by employing the Tsiolkovsky rocket equation:

$$\Delta V = g_0 I_{sp} \ln\frac{m_0}{m_1} \tag{24}$$

where g_0 is acceleration due to Earth's gravity at the surface, I_{sp} is the specific impulse of the propellant being used, and $\frac{m_0}{m_1}$ is the ratio of the fuelled mass to dry mass of the spacecraft. The resulting cost informs the algorithm that there is a value to arriving sooner than later. There are other values to time that are not considered, for instance, it may be desirable to rendezvous sooner to save on operator costs or to meet a specific deadline. These can be implemented on future missions if desired.

To determine the optimal return trajectory, the cost function Equation (20) is repeated many times over two dimensions: relative semi-major axis and time, and the minimum value taken. First, the absolute and relative

states of the deputy spacecraft are determined over a long period of time, propagating the initial conditions forward assuming no thrusts occurred. Then, once for each day, the cost function is computed over a conservatively wide range of semi-major axes. This is done because the eccentricity/argument of perigee saving fraction is a function of the mean argument of perigee at the time of the return trajectory burns, which at times can vary significantly over a period of just a few days (see Figure 4). Therefore, there are times when waiting before performing the return trajectory burn will save fuel overall, even though there may be an additional time cost.

Final Rendezvous and Station Keeping

Near the end of the drift recovery coast phase, the deputy spacecraft must perform manoeuvres to arrest the drift rate between the spacecraft and ease itself in to its station. Applying these impulses at the proper time is crucial to ensuring the spacecraft can rendezvous safely and timely. This requires the definition of a final target relative distance, and a desired safety buffer time.

The final target relative distance is the distance between the spacecraft when rendezvous is considered complete; in the case of CanX-4&5, the inter-satellite link (ISL) has a design range of 5 km, and the spacecraft are considered to be dangerously close to one another at a range of less than 1 km. Therefore, 3 km was chosen as the nominal target distance.

The safety buffer time is the maximum amount of time that the spacecraft can be allowed to drift out of control at any point in time during the drift recovery phase without a risk of collision, and is chosen based on the worst-case expected ground station outage, with an extra buffer to account for a simultaneous unscheduled spacecraft reset. A value of 3 days was found to give reasonable results.

An additional consideration is the time required to arrest the relative drift; with a very powerful propulsion system this would not be required however the maximum impulse limit placed on CNAPS means that the drift arrest will likely require more than one orbit. Time to complete the arrest is calculated as:

$$t_{arrest} = \frac{\Delta V_{a,i_2}}{\Delta V_{orbit,max}} \frac{2\pi}{n}$$
$$\Delta V_{orbit,max} = \frac{2I_{max}}{m_{wet}} \quad (25)$$

where t_{arrest} is the time needed to arrest the drift, $\Delta V_{orbit,max}$ is the maximum velocity change that can occur per orbit, m_{wet} is the spacecraft wet mass, and I_{max} is the maximum commandable impulse. Note that $\Delta V_{orbit,max}$ includes a factor of 2 in the numerator because two thrusts are planned to occur each orbit, 180 degrees apart.

The secular along-track drift rate as a function of the relative semi-major axis is found by solving Equation (9). Then, the angular separation corresponding to when the first rendezvous deceleration thrust should occur can be calculated as:

$$\alpha_0 = \delta\dot{\lambda}\left(t_{buffer} + \frac{t_{arrest}}{2}\right) + \alpha_1 \quad (26)$$

where α_0 and α_1 are the angular separations of the chief and deputy at the start and end of rendezvous deceleration, respectively, and t_{buffer} is the previously described buffer time accounting for ground station outage and spacecraft reset. To find α_1 from a linear distance, the law of cosines is employed:

$$\alpha_1 = \cos^{-1}\left(\frac{-c^2 + a_c^2 + a_d^2}{2a_c a_d}\right) \quad (27)$$

where a_c and a_b are the semi-major axes of the chief and deputy, respectively, and c is the desired linear distance between the spacecraft at the end of rendezvous, 3 km in this case.

The algorithm controlling both the rendezvous drift-arrest and stationkeeping portions of flight were combined as they served a common purpose: choose a relative semi-major axis to bring the spacecraft to a safe relative mean anomaly while ensuring that a loss of control for the buffer time t_{buffer} would not allow the relative range to become dangerously small, and holding the other relative orbital elements as close to zero as possible.

To define the rendezvous drift-arrest trajectory, the following exponential relationship is used:

$$\Delta r_t = \Delta r_0 e^{-\tau t} \quad (28)$$

where e is the base of the natural logarithm, Δr_t is the linear separation between the chief and deputy at time t after the start of the rendezvous arrest phase, Δr_0 is their separation at the start of rendezvous, and τ is the time constant defining the speed of the rendezvous. An ideal rendezvous trajectory would consist of a constant thrust decelerating the spacecraft in to their final relative resting point, however in reality most spacecraft thrusts are impulsive and require operator time to plan, upload, and verify. Therefore, a real rendezvous consists of a series of thrust groups, with each group separated by a

user-defined length of time, which will be denoted by $t_{f,sep}$. For CanX-4&5, two days separated each rendezvous thrust group, with every other day used to analyze the effectiveness of the preceding thrust group. Then, the time constant τ can be defined:

$$\tau = -\frac{\ln\left(1 - \left(-\frac{t_{f,sep}}{t_{buffer} + t_{f,sep}}\right)\right)}{t_{separation}} \quad (29)$$

For example, with a $t_{f,sep}$ of 2 days, and a t_{buffer} of 3 days, τ is about 0.255. That means that every $\tau^{-1} = 3.92$ days, a factor of the distance between the spacecraft changes by a factor of $e^{-1} = 0.368$.

To plan each bidaily thrust group, a target relative semi-major axis for the next leg of the rendezvous must be found. First, the separation of the two spacecraft at the expected time of the thrusts is found by querying the Chief and Deputy states from the simulation. This separation is compared to the target separation after another $t_{f,sep}$ days have elapsed, defining a constant linear velocity, which can be converted to an angular velocity with Equation (27). Substituting the result in to Equation (9) yields the target relative semi-major axis. Then, the target inclination to control the nodal precession is found using the same procedure as before.

Station keeping is similar to rendezvous, except that the use case is somewhat different. Rather than the two spacecraft quickly converging, starting at a predetermined and relatively large distance from one another, station keeping is entered each time a formation concludes, to bring the spacecraft back to a safe state, without any desire to do so quickly. Therefore, rather than a custom time constant, a time constant of 1/6 is typically applied, as this allows the Deputy to reach the target point within a reasonable 5 days of a formation ending, although this can be customized.

Comparison to other Impulsive Control Schemes

The controller described above was compared to the four-thrust controller in [10], as it was relatively simple to implement, and it had also been compared to the controller described in [11]. When given random relative trajectories to correct, DRASTK was found to use an average of 54.6% as much fuel as the four-thrust controller. This compared well to the controller described in [11], which used 51% as much fuel as the four-thrust controller. However, it was found that a large source of error in the four-thrust controller could be attributed to large manoeuvres (>1 m/s) invalidating the assumption of constant eccentricity in Gauss' variational equations; that is, inspecting Equation (16), if the eccentricity changes considerably during a thrust, the linearity of this equation is no longer valid. By simply reducing the maximum manoeuvre magnitude to something smaller (0.25 m/s was used), DRASTK used 76.1% as much fuel as the four-impulse controller.

In some instances, the four-thrust controller performed better than DRASTK, so further optimization is possible. Combining the two controllers and taking the cheaper result uses 71.9% of the fuel of the four-impulse controller alone.

III. COLLISION AVOIDANCE AT EXTREMELY CLOSE RANGE

Between formations, a significant amount of time may be spent keeping station, with the deputy held at a predetermined range from the chief. Ideally, no control thrusts would be necessary to maintain that state; however errors in orbital knowledge and control, differential drag, and other effects will cause the deputy to be perturbed either towards or away from the chief. If left uncontrolled, these perturbations could result in the spacecraft coming undesirably close to one another or even colliding. In particular, following the 100 and 50 m PCO formations, the spacecraft exit the formation in very close proximity to one another, in orbits that could cross given a small disturbance force. Detrimental effects to the spacecraft can occur even if no contact is made during a close approach; at extremely close range, the ISL radios can become saturated and damaged. An additional buffer is also desirable to account for model and control errors.

Nominally, to maintain a spacecraft separation of 1 to 2 km, small, occasional (on the order of every 2 or 3 days) thrusts are sufficient to overcome the largest of errors and perturbations. However, additional confidence can be gained by putting the deputy in to a passively safe relative orbit, where the deputy's orbit never crosses the chief's. This is done by applying a velocity change to the deputy, in two directions perpendicular to the chief's velocity vector, 90 degrees out of phase with one another.

At these ranges (~5 km or less), it becomes intuitively useful to describe relative spacecraft motion in Cartesian coordinates, centred on the Chief, or reference, spacecraft. For this, the Local-Vertical, Local-Horizontal (LVLH) frame is used [12]. In this frame the X-axis is parallel to the spacecraft's position vector relative to the Earth's centre of mass and is known as the "radial" direction, the Y-axis is parallel to the spacecraft's instantaneous velocity vector and is known as the "along-track" direction, and the Z-axis

completes the triad, pointing perpendicular to the orbital plane and is known as the "cross-track" direction.

The previously mentioned directions perpendicular to the velocity vector are then the radial and cross-track directions. As sinusoidal motions with a common period of 1 orbit, it should be possible to phase them such that the trajectory of one spacecraft never intersects the other one, instead tracing out a spiral around its companion's orbit (see Figure 5). Note that throughout this section, to be more general, the deputy will be referred to as the "perturbed spacecraft" and the chief as the "reference spacecraft".

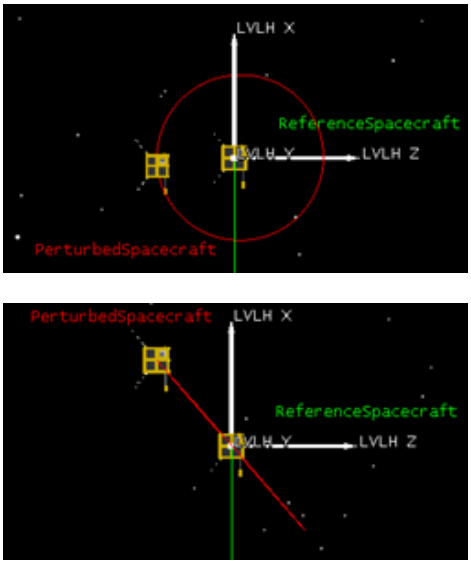

Figure 5: Passively safe (top) and unsafe (bottom) relative motion, as viewed from along the reference spacecraft's velocity vector.

To describe the motion in this frame, the Hill-Clohessy-Wiltshire (HCW) equations can be used. These equations describe relative spacecraft motion, with the assumption that the orbits are circular, the spacecraft are relatively close, and short periods of time are used [13]. They are written as:

$$\begin{bmatrix} x(t) \\ y(t) \\ z(t) \\ \dot{x}(t) \\ \dot{y}(t) \\ \dot{z}(t) \end{bmatrix} = \begin{bmatrix} 4-3c & 0 & 0 & \frac{s}{n} & \frac{2}{n}(1-c) & 0 \\ 6(s-nt) & 1 & 0 & -\frac{2}{n}(1-c) & \frac{4s-3nt}{n} & 0 \\ 0 & 0 & c & 0 & 0 & \frac{s}{n} \\ 3ns & 0 & 0 & c & 2s & 0 \\ -6n(1-c) & 0 & 0 & -2s & 4c-3 & 0 \\ 0 & 0 & -ns & 0 & 0 & c \end{bmatrix} \begin{bmatrix} x_0 \\ y_0 \\ z_0 \\ \dot{x}_0 \\ \dot{y}_0 \\ \dot{z}_0 \end{bmatrix} \quad (30)$$

$$c = \cos nt$$

$$s = \sin nt$$

The process of entering a passively safe relative orbit can be summarized by the following:

1. Identify the current relative motion
2. Identify the desired relative motions
3. Locate the intersection of 1) and 2)
4. Choose the intersection that requires the smallest change in velocity
5. Perform thrust

Table 1 gives the initial conditions for an example of an unsafe motion, at 04:05:00 UTC. Using Equation (30), this can be propagated through time to yield the graph in Figure 6. Note how both the radial and cross-track motions cross zero only a few minutes apart. With only a small perturbation, these spacecraft could collide.

Table 1: Initial conditions of an unsafe motion

Vector	Perturbed spacecraft (LVLH frame)
x (m)	-36.78
y (m)	8.76
z (m)	30.34
ẋ (mm/s)	-2.15
ẏ (mm/s)	79.53
ż (mm/s)	-19.16

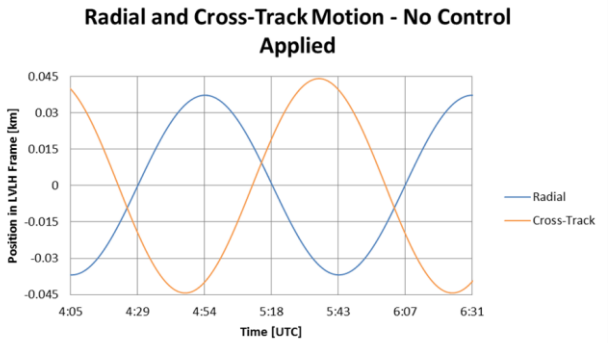

Figure 6: Example of passively unsafe motion

With the uncorrected motion identified, the next step is to determine what the desired motion looks like. Let the requirement be that the two spacecraft maintain at least 30 m separation at all times. The phase of one of these motions needs to be changed to be out of phase with the other. In this example, the radial motion will be held constant, and the cross-track motion will be controlled. Though not necessary, the amplitude of the cross-track motion will also be altered to match the radial motion. Then, to define the desired motion, the speed and displacement of the cross-track motion needs to be defined at one point in time. An easy point to use is when the radial motion crosses zero, at which time the cross-track displacement should be at its maximum and its speed should be zero. Solving Equation (30), this occurs 1498 seconds after the initial state, at 04:29:58. At that time, the uncorrected cross-track displacement is -19.63 m and the uncorrected velocity is -42.65 mm/s. Setting the desired cross-track displacement to 37 m and velocity to 0, and setting the initial time to 04:29:58, the two cross-track motions are:

$$z_0(t) = z_0(0)\cos nt + \frac{\dot{z}_0(0)}{n}\sin nt$$
$$z_1(t) = z_1(0)\cos nt + \frac{\dot{z}_1(0)}{n}\sin nt \quad (31)$$

where the 0 and 1 subscripts refer to the uncorrected and desired states, respectively. Their intersection is found by solving for t:

$$t_i = \frac{\operatorname{atan}\left(n\frac{z_1(0) - z_0(0)}{\dot{z}_0(0) - \dot{z}_1(0)}\right)}{n} \quad (32)$$

where t_i is the time of intersection. Solving this gives an intersection at -894 seconds, at 4:15:04. Again from Equation (30):

$$\dot{z}_0(t) = -z_0(0)n\sin nt + \dot{z}_0(0)\cos nt$$
$$\dot{z}_1(t) = -z_1(0)n\sin nt + \dot{z}_1(0)\cos nt \quad (33)$$

the velocity difference, which dictates the magnitude of the manoeuvre impulse, is the difference between these two values at the intersection time:

$$\Delta V_z = n\sin nt_i\,(z_0(0) - z_1(0)) + \cos nt_i\,(\dot{z}_1(0) - \dot{z}_0(0)) \quad (34)$$

Solving this yields a velocity change of -7.42 cm/s. While this is one solution to the problem, another exists, 180 degrees out of phase from this one. By setting the desired cross-track displacement to -37 m at the initial time and repeating the procedure, an intersection is found at 384 seconds, 04:36:22, and ΔV_z with a velocity change of only 4.65 cm/s. Selecting the smaller thrust, the result can be seen in Figure 7.

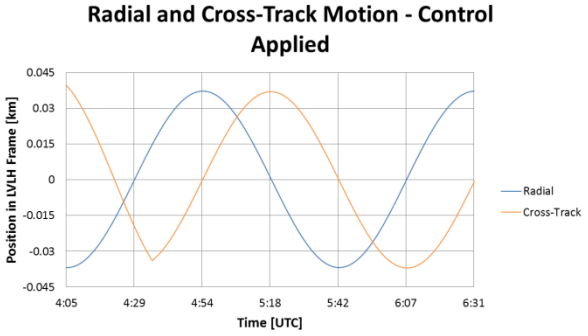

Figure 7: Radial and cross-track motion after performing the control manoeuvre at 04:36:22

IV. ON-ORBIT RESULTS

CanX-4 and CanX-5 were launched from the Satish Dhawan Space Centre on 30 June, 2014 04:22 UTC aboard the Indian Space Research Organization (ISRO) PSLV-C23. The launch vehicle's primary payload was the French SPOT-7 Earth observation spacecraft. Two other microsatellites were also carried aboard. The satellites were released in to a circular 650 km sun-synchronous orbit over the Indian Ocean.

Figure 8: PSLV-C23 lifting off from the Satish Dhawan Space Centre.

Drift Recovery

CanX-4 and CanX-5 were mounted on to the PSLV launch vehicle using separate XPODs. The original design had the spacecraft ejected together from a single XPOD, and only separated once they had been fully commissioned and could be quickly brought in to stable relative orbits; however launch vehicle constraints prevented this. Therefore, it became very important that at least one spacecraft, the deputy, become fully commissioned quickly, in order to begin arresting their relative drift. Nominally, CanX-4 has been assigned as the chief, and CanX-5 as the deputy.

Table 2: Differential mean orbital elements of CanX-5 to CanX-4 immediately after launch.

Differential Mean Elements	Value
Semi-major axis	-708 m
Inclination	-2.32×10^{-3} °
Eccentricity	-1.75×10^{-4}
RAAN	-1.51×10^{-3} °
Argument of Perigee	55.2°
Mean Anomaly	-57.6°

From GPS data post-processed on the ground, the relative mean orbital elements immediately after launch vehicle kick-off were determined and can be seen in Table 1. With a relative semi-major axis of -708 m, the spacecraft were drifting apart at about 95 km/day.

These relative states were input to the DRASTK program, which determined that the fuel optimal trajectory, after the deputy was fully commissioned, required the relative semi-major axis and inclination to be changed to 306 m and 0.00129° respectively, 26 days

after launch. The total cost, including fuel lost to leakage, would be about 1.9 m/s, and rendezvous would occur in early October.

During the thrusts to put the Deputy on to the return trajectory, it was discovered that the propulsion system was performing near its theoretical maximum, exceeding expectations by ~20%. This, combined with knowledge that drift recovery could be completed for far less than the 5 m/s that was originally budgeted, meant that a considerable amount of margin was available to use. Therefore, the decision was made to increase the speed of drift recovery such that station keeping would be entered around 4 September, at an additional cost of about 29 cm/s. Thus, the return trajectory was altered to a relative semi-major axis of 720 m and relative inclination of 0.00300°.

On 16 August, the spacecraft reached a relative range of 315 km, from a maximum of 2300 km on 25 July (see Figure 9). At this point, deceleration thrusts began, such that the spacecraft maintained a minimum separation of 3 days for safety. Control thrusts were applied every 2 days, which was a compromise between thrusting every day, which would allow slightly faster recovery, and thrusting less often which requires less operator time. Using this method, the Deputy stayed within 12 km of the reference trajectory. That error dropped to less than 2 km when the spacecraft were 15 km or closer. The process took about 17 days. When the final drift arresting thrust was sent on 2 September, the spacecraft were within 50 m of their nominal parking positions with nearly zero residual relative orbital elements (see Table 3).

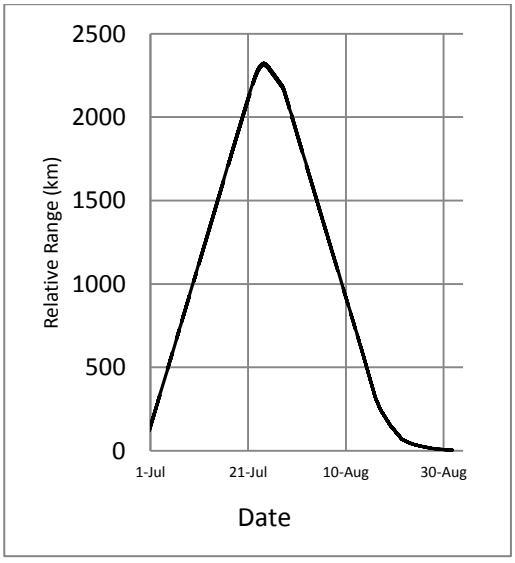

Figure 9: Relative range of the two spacecraft during drift recovery

Table 3: Differential Mean orbital elements of CanX-5 to CanX-4 after completing drift recovery.

Differential Mean Elements	Value
Semi-major axis	0.5 m
Inclination	1×10^{-6} °
Eccentricity	8×10^{-7}
RAAN	1.3×10^{-6} °
Argument of Perigee	0.014°
Mean Anomaly	0.009°
Range	2.95 km

Total ΔV expended in manoeuvres during drift recovery is predicted to have been 2.03 m/s over 102 individual manoeuvres, based on the best estimates of on-orbit thruster performance. Based on simulations done on the ground, assuming no attitude or navigational errors, the minimum cost to perform these manoeuvres would be 1.92 m/s. The error, 5.7%, is well within expectations from simulations, where mean errors were found to be 5.8% with a standard deviation of 2.7%.

Of the 2.03 m/s spent on drift recovery manoeuvres, approximately 1.102 m/s was used adjusting the semi-major axis and inclination to begin drift recovery, 0.284 m/s was used fixing the eccentricity and argument of perigee, 0.038 m/s was used performing a small course correction manoeuvre, and 0.611 m/s was spent decelerating in to station keeping. Had the first set of thrusts not also been used to change the eccentricity and argument of perigee in a beneficial direction as described earlier, simulations estimate that it would have cost 0.60 m/s more to correct those elements.

Station keeping took place between the end of drift recovery on 2 September and the completion of the primary mission on 19 November 2014. The total fuel usage during that time amounted to 0.810 m/s over 59 thrusts. Most of this fuel was used to correct large relative drifts between formations, and entering passively safe relative orbits after the projected circular orbit formations.

VI. NEXT STEPS

The CanX-4&5 mission was accomplished in November 2014 with the successful completion of its four primary formation experiments. As of April 2015, the spacecraft are drifting idle, though nearly two-thirds of the total system fuel remains for additional experimentation.

Future work on the DRASTK controller will focus on further optimizing the controller to account for higher order orbital perturbations, as well as increased modularity and user accessibility to allow the system to

be applied to future constellation and formation missions.

VII. CONCLUSIONS

A system for drift recovery and station keeping was designed, implemented, and executed on-orbit. This system included algorithms to compute fuel efficient return trajectories for separated spacecraft, as well as a controller to put the spacecraft on that trajectory, make mid-course corrections, and stop at the target range, as well as a user interface to simplify operations. A method to allow passively safe operations at extremely close ranges was also tested and executed on-orbit. The results were found to compare favourably to previous works in this field, and met all requirements. Drift recovery of the CanX-4&5 system was completed using 2.032 m/s of ΔV. Navigational and attitude errors were predicted to cause an increased fuel cost of about 5.75% during the drift recovery phase, and the on-orbit estimate of 5.72% came very close to matching this. In particular, this work will benefit the future implementation of constellation maintenance and orbit phasing controllers.

VIII. ACKNOWLEDGMENTS

The author would like to acknowledge the contributions of many SFL staff and students, past and present, who have contributed to this mission over the years. In particular, they would like to thank the SFL ground station team for their assistance, and the CanX-2 and BRITE mission operations teams for their cooperation. They would also like to acknowledge the research contributions of Dr. Christopher Damaren at the University of Toronto, and Dr.. Elizabeth Cannon at the University of Calgary.

The following sponsors of the CanX-4&-5 program are gratefully acknowledged:

- Canadian Space Agency
- Defense Research and Development Canada (Ottawa)
- Natural Sciences and Engineering Research Council of Canada (NSERC)
- Ontario Centers of Excellence (OCE)
- MDA Space missions
- Sinclair Interplanetary

[1] K. Sarda, C. C. Grant, S. Eagleson, D. D. Kekez and R. E. Zee, "Canadian Advanced Nanospace Experiment 2 Orbit Operations: Two Years of Pushing the Nanosatellite Performance Envelope," in *European Space Agency Small Satellite Systems and Services Symposium*, Funchal, 2010.

[2] S. Bandyopadhyay, G. P. Subramanian, R. Frost, D. Morgan and F. Y. Hadaegh, "A Review of Impending Small Satellite Formation," in *53rd AIAA Aerospace Sciences Meeting*, Kissimmee, 2015.

[3] A. M. Beattie, K. Sarda, D. D. Kekez, R. E. Zee and B. T. Narhein, "AISSAT-1 In-Orbit Verification of the Generic Nanosatellite Bus," in *Proceedings of the 62nd International Astronautics Congress*, Toronto, 2011.

[4] N. Orr, J. Ever, B. Larouche and R. E. Zee, "Precision Formation Flight: The CanX-4 and CanX-5 Dual Nanosatellite Mission," in *20th Annual AIAA/USU Conference on Small Satellites*, Logal, Utah, 2007.

[5] B. Risi, "The CanX-4 and CanX-5 Formation Flying Mission," in *27th Annual AIAA/USU Conference on Small Satellites*, Logan, 2013.

[6] A. H. J. de Ruiter, Orbital Mechanics, Ottawa, 2011.

[7] K. T. Alfriend and H. Schaub, "Dynamics and Control of Spacecraft Formations: Challenges and Some Solutions," *Journal of the Astronautical Sciences*, vol. 48, pp. 249-267, April-Sept 2000.

[8] Y. Kozai, "The Motion of a Close Earth Satellite," *The Astronomical Journal*, pp. 367 - 377, 1959.

[9] H. Schaub and J. L. Junkins, Analytical Mechanics of Space Systems 2nd Edition, AIAA, 2009.

[10] H. Schaub and K. T. Alfriend, "Impulsive Feedback Control to Establish Specific Mean Orbit Elements of Spacecraft Formations," *Journal of Guidance, Control, and Dynamics*, vol. 24, no. 4, pp. 739-745, 2001.

[11] L. Breger and J. P. How, "Gauss' Variational Equation-Based Dynamics and Control for Formation Flying Spacecraft," *Journal of Guidance, Control, and Dynamics*, vol. 30, no. 2, pp. 437-448, 2007.

[12] D. A. Vallardo, Fundamentals of Astrodynamics and Application, Third Edition, Hawthorne: Microcosm Press, 2007.

[13] S. R. Ploen, D. P. Scharf, F. Y. Hadaegh and A. B. Acikmese, "Dynamics of Earth Orbiting Formations," Jet Propulsion Laboratory, Pasadena, 2004.

[14] S. Eagleson, K. Sarda, A. Philip and J. Hrzymisch, "Attitude Determination and Control: CanX-4/-5," SFL-Internal Document, 2007.

[15] N. Roth, "CanX-4 & CanX-5 Long-Term Drift Recovery Strategy," UTIAS-SFL, Toronto, 2011.